Photoelectron diffraction in the x-ray and ultraviolet regime: Sn-phthalocyanine on Ag(111)

Greif, M ; Castiglioni, L ; Seitsonen, Ari P ; Roth, S ; Osterwalder, J ; Hengsberger, M

DOI: https://doi.org/10.1103/PhysRevB.87.085429

Photoelectron Diffraction in the X-Ray and Ultraviolet Regime: Sn-Phthalocyanine on Ag(111)

Michael Greif[1], Luca Castiglioni[1], Ari P. Seitsonen[2], Silvan Roth[1], Jürg Osterwalder[1], and Matthias Hengsberger[1]
[1] *Institute of Physics, University of Zürich, Winterthurerstrasse 190, 8057 Zürich, Switzerland and*
[2] *Institute of Physical Chemistry, University of Zürich, Winterthurerstrasse 190, 8057 Zürich, Switzerland*
(Dated: December 20, 2012)

The bonding geometry of tin-phthalocyanine (SnPc) on Ag(111) has been studied using x-ray and ultraviolet photoelectron diffraction (XPD and UPD, respectively). Experimental diffraction patterns were compared to single-scattering-cluster calculations. XPD data could be well reproduced by the simulations and allowed for the determination of several structural parameters. At a coverage of 0.9 ML all molecules are in a "tin-down" configuration and the non-planar shuttlecock-shaped SnPc molecule undergoes flattening upon absorption on Ag(111). UPD data from the second highest occupied molecular orbital (HOMO-1) turn out to be highly sensitive to minor structural changes, including also the vertical distance between tin atoms of the SnPc and the surface layer of the substrate, which is found to be 2.3 Å. We thus demonstrate how UPD can complement the well-established XPD method and discuss remaining challenges in the theoretical description of photoelectron diffraction from molecular orbitals at low energies. The UPD method is particularly attractive in view of the increasing availability of ultrashort pulsed laser sources in the XUV regime, which could enable pump-probe experiments with high structural sensitivity.

I. INTRODUCTION

Photoelectron diffraction is a well established method to probe the structure of various types of surfaces such as clean metal surfaces, ultra-thin epitaxial films or atomic and molecular ad-layers adsorbed on metal surfaces.[1] X-ray photoelectron diffraction (XPD) has been successfully used for more than 20 years to image near-surface crystal structures[2] or adsorption geometries of molecules with atomic resolution.[3] The mechanisms of core-level photoemission and final state scattering and diffraction exploited in XPD are largely understood. The means to analyze diffraction patterns of photoelectrons with much lower kinetic energies, such as photoelectrons excited by ultraviolet light, are much less explored. Enhanced backscattering in ultraviolet photoelectron diffraction (UPD) leads to stronger contributions of additional scattering pathways, thereby promising to deliver even more information than XPD. This comes at the cost of more complex diffraction patterns which are further complicated by dominating interference effects, while in XPD the presence of strong forward scattering enhancements often provides a direct fingerprint of the arrangement of atoms in the near-neighbor shells of a photoemitter.[2] The currently largest obstacle to overcome, however, comes from the fact that UV-excited photoelectron spectra are typically restricted to emission from valence states and molecular orbitals, where an accurate theoretical description of the photoemission process and the final state scattering is only just emerging.[4] A combination of photoelectron diffraction with newly available pulsed light sources in the UV-XUV regime, *e. g.* via high harmonics generation (HHG),[5] could lead to a powerful method to study structural dynamics at the atomic scale with femtosecond temporal resolution. We demonstrate in this work that UPD can indeed be used to retrieve structural parameters of a complex molecular adsorbate system and that the interference patterns are sensitive to even very small structural changes.

To record XPD or UPD patterns, the photoelectron intensity of a selected state is mapped as a function of emission angles over a large part of the hemisphere above the sample. This measurement approach has recently also been used to obtain UPD patterns from molecular orbitals in order to perform orbital tomography of organic molecules on surfaces.[6–8] In these studies the spatial distribution of the electronic wavefunction is calculated via a 3-D Fourier transformation of the measured photoelectron intensity distribution. We present another approach to interpret such measurements based on scattering-cluster calculations.[9] Such calculations have proven their value in modeling XPD patterns of core level emission of adsorbates[3] and of pristine metal surfaces,[2] even at the single-scattering cluster (SSC) level. The SSC formalism was also successfully applied to the modeling of d-band integrated UPD measurements of Cu valence states,[10] where the scattering approach was recently further validated by multiple scattering methods.[11]

We have chosen tin-phthalocyanine (SnPc) adsorbed on Ag(111) as a model system to demonstrate the sensitivity of a combined XPD/UPD study to structural parameters and potentially to structural dynamics. It represents a sufficiently complex system that has been studied extensively by other methods in the last few years. Comprehensive work by Stadler *et al.*[12,13] using photoelectron spectroscopy, x-ray standing wave (XSW) measurements as well as LEED studies shows that SnPc adsorbs in the monolayer with the molecules lying flat on the Ag(111) surface. At sub-monolayer coverage the adlayer has different structural phases, which are associated with a conformational change of the SnPc molecule. Conformations with the Sn atom on top of the molec-

ular plane ("tin-up") or with the Sn atom beneath the molecular plane ("tin-down") were identified. The different geometrical phases can be tuned via temperature and coverage. The mechanisms driving those phase transitions are intermolecular attraction and repulsion due to charge transfer between the chemisorbed molecular monolayer and the silver substrate.[12] While DFT calculations for the molecule in the gas phase predict a non-planar, shuttlecock-shaped structure, XSW measurements as well as density functional theory (DFT) calculations[14] show that the molecules undergo a flattening upon adsorption. Additional photoelectron spectroscopy studies yielded insights into the electronic structure of the system.[15] Other experiments employing scanning tunneling microscopy (STM)[16,17] added further geometrical information about this system, such as the rotational orientation of the molecules with respect to the substrate surface. A recent DFT study investigated how the highest occupied molecular orbitals (HOMO) are involved in the bonding mechanism of the SnPc to the metal substrate.[14] It was found that the second highest occupied molecular orbital (HOMO-1) plays an important role in the chemical bonding of molecules and substrate.

In the first part of this work we present XPD measurements of core levels of the molecular tin atom. Geometrical parameters obtained from these measurements and further parameters drawn from literature serve as a reference to analyze and interpret the more complex UPD patterns in the second part of this paper. In the UPD measurements emission from the HOMO-1 orbital of SnPc was recorded. This study shall demonstrate the high sensitivity of UPD to electronic and structural parameters.

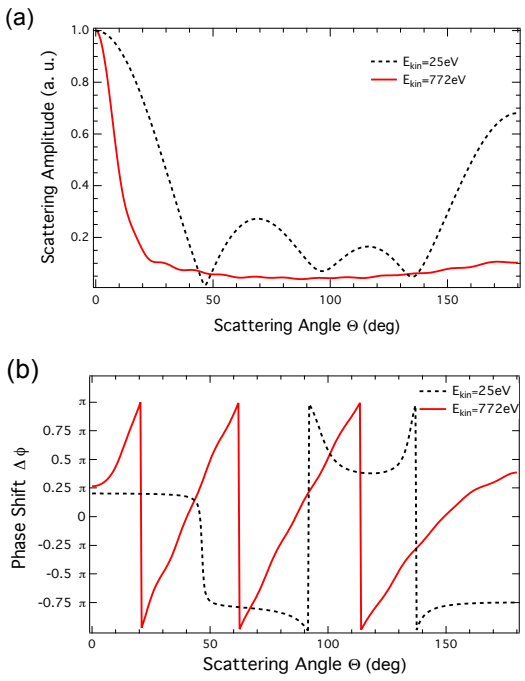

FIG. 1. (a) Calculated angular dependence of the scattering amplitude for electrons being scattered at an Ag atom. The red trace corresponds to electrons excited from Sn $3d_{5/2}$ states with Mg K_α light of $h\nu = 1253.6$ eV photon energy. The black dashed trace represents electrons excited from the HOMO-1 of SnPc with a He I_α source ($h\nu = 21.21$ eV). (b) Phase shifts for an electron wave due to the scattering process at an Ag-atom. Again red and black dashed traces represent photoelectrons with the corresponding kinetic energy as in the upper picture. Note that the energies given in the the legend are kinetic energies inside the solid.

II. METHOD

To analyze the measured photoelectron diffraction data, they are compared to SSC calculations. In the SSC approach the photoemission intensity $I(\mathbf{k}_f)$ depending on the final state wave vector $\mathbf{k}_f$ is expressed as the coherent sum of the direct wave emitted from a localized core level and all singly scattered waves from a cluster of atoms surrounding the photoemitter, evaluated at the spot of detection in the far field. On their way to the detector the direct and scattered waves have different pathways but a fixed phase relation. The photoelectron intensity distribution in k-space is given by[9]

$$I(\mathbf{k}_f) \propto \Big| m_{if}(\mathbf{k}_f) e^{-L_0/2\lambda_i} + \sum_j m_{if}(\mathbf{r}_j) e^{-L_j/2\lambda_i} \times \frac{f_j(\theta_j)}{r_j} e^{ik_f r_j(1-cos\theta_j)} \cdot W_j \Big|^2 + TDS. \quad (1)$$

L_0 and L_j indicate the path lengths of the respective waves inside the surface, λ_i is the inelastic mean free path, $f_j(\theta_j)$ is the complex atomic scattering factor (containing also the scattering phase shift) depending on the scattering angle θ_j of the j-th scatterer and $\mathbf{r}_j$ the vector to the j-th scatterer. The index j runs over all atoms within a limited cluster of atoms, excluding the photoemitter. The Debye-Waller factor W_j and TDS (thermal diffuse scattering term) both describe effects due to thermal disorder.[9] While the initial state is considered to be an atomic core state, the final state is a singly scattered state. The different pathways imply primary photo-excitation into different directions, therefore each is multiplied with the corresponding photoemission matrix element[1]

$$m_{if}(\mathbf{k}) = \langle \phi(\mathbf{k}) | \boldsymbol{\varepsilon} \cdot \boldsymbol{k} | \psi_{nlm} \rangle \quad (2)$$

between the initial core state ψ_{nlm} and a final state $\phi(\mathbf{k})$, where both are approximated by considering the case of a free atom. In Eq. 2 the variable $\mathbf{k}$ describes either the propagation direction of the direct wave ($\mathbf{k}_f$) or the propagation towards the scatterer $\mathbf{r}_j$. $\boldsymbol{\varepsilon}$ is the polarization vector of the incident light and $\boldsymbol{\varepsilon} \cdot \boldsymbol{k}$ is the unit dipole operator in direction of the outgoing wave.

Upon switching from XPD to UPD, *i.e.*, to photoelec-

trons with lower kinetic energies ($E_{kin} < 50$eV), the scattering behavior changes. Figs. 1(a) and (b) show amplitude and phase of the complex scattering factor $f_j(\theta_j)$ for fast electrons excited with x-rays from Sn 3d core states and for slow electrons excited with He I_α light from a molecular orbital. The slow electrons have a higher probability to be scattered to larger angles, including 180° backscattering by the Ag substrate, while faster electrons are scattered predominantly into the forward direction. Also the phase shifts to the photoelectron waves caused by the scattering events are large for backscattered electrons in the low energy case. Hence diffraction patterns recorded for photoelectrons in the UPD regime show strong interference effects and additional backscattering signals.

The scattering phase shifts that are required to compute the coherent sum in Eq. 1 were calculated employing the muffin tin potential approximation[18] with atomic wave functions taken from literature.[19] Radial transition matrix elements and the transition phase shifts where either taken from literature[20] or calculated with the PSRM code by Chen and van Hove.[21] Furthermore the scattering amplitudes and phases shown in Fig. 1 were obtained by calculating the scattering of a plane wave off a radially symmetric potential representing an isolated Ag atom.

III. EXPERIMENTAL

All experiments were carried out in a modified VG ESCALAB 220 photoemission spectrometer at a base pressure of $p = 1 \cdot 10^{-10}$ mbar.[22] As light sources the He I_α (photon energy $h\nu = 21.21$ eV) and the Mg K_α ($h\nu = 1253.6$ eV) lines were used. All measurements were performed at room temperature. Fig. 2 illustrates the geometry of the experimental setup.

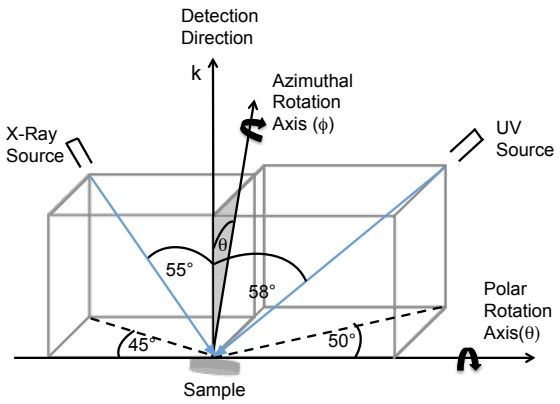

FIG. 2. Sketch of the measurement geometry in the experimental XPD/UPD setup. The incident light has a fixed direction with respect to the detection direction. The sample can be rotated about the polar rotation axis and the azimuthal rotation axis, as indicated by the curved arrows.

A. Preparation

The Ag(111) substrate was cleaned with several sputtering and annealing cycles to prepare a clean and well ordered surface. The surface quality was then checked by XPS, UPS, and LEED. SnPc films were prepared at room temperature from resublimed SnPc powder evaporated from a self-made Knudsen cell. The pressure during the preparation was below $1 \cdot 10^{-8}$ mbar. After evaporation the sample was annealed for five minutes at a temperature of 150°C. As indication for sufficient annealing we made sure that the adsorbate superstructure was homogeneous over the sample by taking LEED pictures from different sample spots. As the superstructure homogeneity was also a crucial criterion in the annealing recipe in Stadler's work,[12] we took the disappearance of multiple superstructures through annealing as a sign that the molecules had gained enough thermal energy to move over terrace steps of the sample and that the sample was sufficiently annealed.

The evaporation rate was calibrated via the phase transition of SnPc at 0.9 ML from the diffuse to the incommensurate superstructure at room temperature, which can be verified by LEED measurements.[12] Additional XPS measurements confirmed the found evaporation rate. This resulted in an accuracy in the SnPc coverage of ±0.05 ML.

B. The System

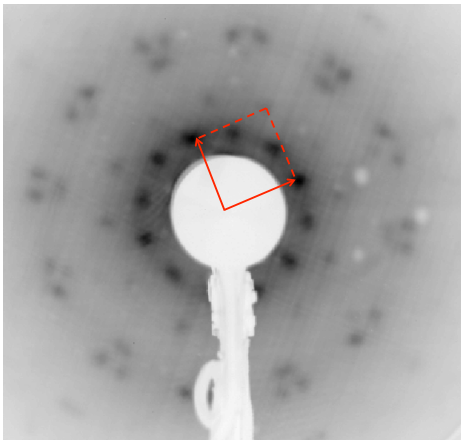

FIG. 3. LEED pattern of 0.9 ML SnPc on Ag(111) recorded at an electron kinetic energy of $E_{kin} = 23$ eV. An incommensurate superstructure of the SnPc molecules with six domains is visible. Note that the substrate 1x1 spots are far outside the presented image frame.

As known from the LEED analysis by Stadler *et al.*,[12] SnPc on Ag(111) has three phases with different superstructures in the single-layer regime. In our work we focus on the incommensurate phase found at 0.9 ML

coverage at room temperature, where all molecules are adsorbed in the "tin-down" conformation. In Fig. 3 we present the LEED data from a representative sample at this particular coverage. The spot pattern consists of six domains: three rotational domains multiplied by two because of an additional mirror symmetry. The superstructure matrix[23] of the individual domains is

$$\begin{pmatrix} 5.64 & 2.66 \\ -0.07 & 4.86 \end{pmatrix}.$$

IV. X-RAY PHOTOELECTRON DIFFRACTION

In this section we present the results of XPD measurements and show how they provide information about the structure of SnPc adsorbed on Ag(111). All XPD measurements were performed with Mg K_α light. The Sn $3d_{5/2}$ core level of the central Sn atom in the SnPc molecule was chosen as emitter, *i. e.* the inelastic background subtracted Sn $3d_{5/2}$ photoemission intensity distribution is measured as a function of emission angles at constant kinetic energy of the electrons.[1] To account for the mostly instrumental polar intensity background, a Gaussian shaped polar background profile was subtracted from every pattern. In Fig. 4 (f) the XPD pattern of 0.9 ML SnPc on Ag(111) is shown: 12 equidistant maxima centered at a polar angle of $\theta = 74°$ are visible (label α). The four-fold symmetry of the individual molecules is not directly reflected in these data. Due to the three-fold rotational symmetry of the substrate the molecules adsorb in three equivalent orientations, leading to this 12-fold arrangement of maxima (see discussion below). Hence the data can be three-fold averaged in order to increase the statistical accuracy of the data. No further symmetrizing was applied. The averaged pattern is shown in Fig. 4 (g). Small variations in the intensities of the 12 maxima remain after the averaging process, hinting at the possibility that the three orientational domains might not be equally populated. This may occur due to a slight miscut of the crystal surface, leading to steps running along preferential directions. More to the center of the three-fold averaged XPD pattern [Fig. 4(g)] weaker features are visible that show a clear three-fold symmetry. The three weak spots at $\theta = 55°$ that are labled with β are exactly at the positions where the substrate XPD pattern of Ag $3d_{5/2}$ (Fig. 4(e)) shows pronounced maxima along the next-nearest-neighbor directions [001], [100], and [010]. They might not be intrinsic to the Sn $3d_{5/2}$ XPD pattern but result from the incomplete subtraction of the spectral background which has imprinted a three-fold diffraction pattern from inelastically scattered photoelectrons from the substrate. The broader signals at similar polar angles are not completely understood and will not be discussed further.

To show how the experimental result can be interpreted we present a series of SSC simulations in Figs. 4 (a) to (c) that show the evolution of the pattern as the cluster is more and more adjusted to match the actual bonding geometry of the SnPc molecules. Figure 4(a) shows the SSC result for a cluster with the atoms of a single free-standing SnPc molecule in the "tin down" conformation, *i.e.* the solid angle covers the hemisphere for positive values of the z coordinate and the Sn-atom is located below the molecular plane in the negative z-direction. The coordinates of the atoms in the cluster are taken from a DFT calculation for a free SnPc molecule. The calculations were performed with TURBOMOLE[24] using the basis set def2-TZVPP and an effective core potential for Sn. The exchange correlation functional was PBE0.[25] In the figure one can see a four-fold symmetric pattern where each of the four pairs of bright maxima at a polar angle of $\theta = 68°$ (label γ) is the result of forward scattering at the two nearest carbon atoms in the pyrrollike ring [see model of molecular structure in Fig. 4 (d)] . Next to each pair, at a slightly lower polar angle, one can see a local intensity maximum resulting from a nearest-neighbor nitrogen atom (label δ). Rotated by an angle of 45° in azimuth are weak structures labeled with ε, each caused by one of the four other nitrogen atoms.

The next step in the series is the simulation with a cluster where the molecule is adsorbed on the Ag(111) substrate [Fig. 4 (b)]. The cluster includes the first two atomic layers of Ag atoms underneath the molecule. XSW data[12] showed that the molecules undergo a conformational change upon adsorption on Ag(111): The slightly shuttlecock-shaped phthalocyanine backbone is flattened and the Sn atom in the center moves closer to the molecular plane. As result an Ag-Sn distance along the z-axis of $d_{Sn-Ag} = 2.25$ Å and a Ag-C distance along the z-axis of $d_{C-Ag} = 3.05$ Å was measured. An illustration of the adsorption geometry is shown in Fig. 5.

In our second simulation [Fig. 4 (b)] we adjusted the molecular geometry to these parameters. As expected, by flattening the molecule the brightest features move towards higher polar angles ($\theta = 76°$), which is close to those found in the experimental data ($\theta = 74°$). This is seen more clearly in Fig. 6, where polar intensity distributions averaged over all azimuthal angles are presented. The measured data are compared to the simulations of the flattened molecule and of the free molecule. The polar position of the experimental maxima is much closer to the simulation performed with the flattened molecule, thus confirming the XSW result.

Since the superstructure of the adsorbate is incommensurate with the substrate periodicity, there is not only a single well-defined adsorption site on the Ag(111) unit cell. The molecules occupy a continuous range of adsorption sites on the surface. To account for this in our calculations we discretized the substrate unit cell into a grid with 20 equidistant adsorption sites and did the calculation as many times, each time with a single molecule adsorbed on a different site. Afterwards we averaged over the outcome of all 20 SSC calculations. The azimuthal orientation of the SnPc molecules with respect to the Ag-substrate in the cluster was chosen as shown in Fig.

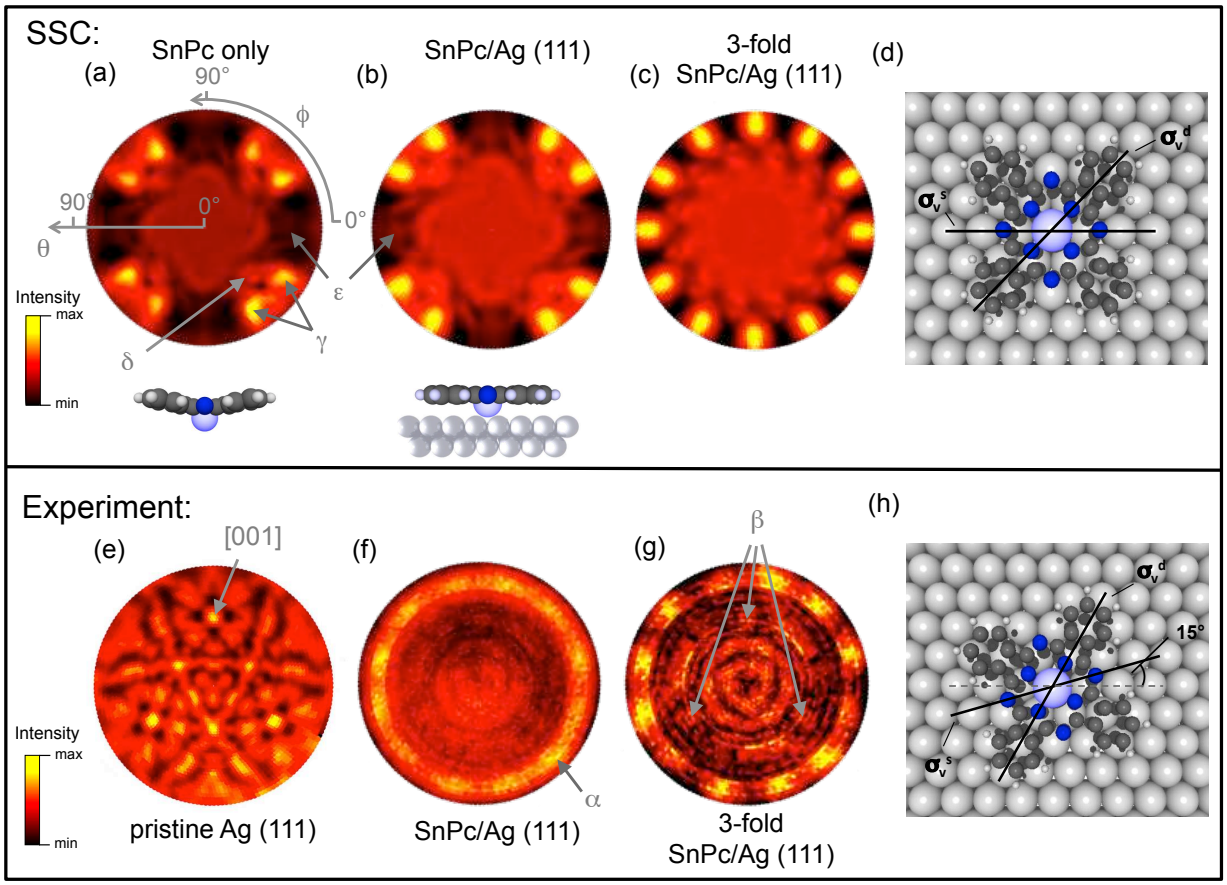

FIG. 4. XPD measurements and corresponding SSC calculations from SnPc/Ag(111). (a) SSC of a non planar free SnPc molecule (molecule shown in the inset below). (b) SSC pattern of an adsorbed molecule in a flattened geometry as taken from Stadler *et al.*[12] (c) three-fold averaged SSC pattern of (b). The experimental pictures show in (e) an XPD pattern of the Ag $3d_{5/2}$ state of the clean Ag(111) substrate, in (f) the inelastic background-subtracted pattern of a 0.9 ML thick film of SnPc on Ag(111) and in (g) the three-fold averaged pattern of (f). All diffraction patterns show a polar range reaching from normal emission in the center of each picture to $\theta_{\max} = 82°$ at the outer border. All patterns were Gaussian background subtracted. With the excepion of (e), the emitter is always the Sn $3d_{5/2}$ core state. Labels α through ε mark selected spots that are referred to in the text. (d) SnPc molecule and its orientation with respect to the Ag-substrate, as it was used in the SSC simulation in (b) and (c). (h) Experimental rotational orientation of the SnPc molecules with respect to the Ag(111) substrate. The diagonal vertical mirror plane σ_v^d of SnPc aligns with the direction of the rows of Ag atoms, and the orientation is thus rotated by 15° with respect to the molecule in (d).

4 (d): the vertical molecular mirror plane σ_v^s is aligned with the unit cell vector of the Ag(111) substrate, *i.e.* along rows of Ag atoms in the surface. As already mentioned in section II, for electrons from the Sn $3d$ core levels with kinetic energies of 772 eV, there are nearly no contributions to the pattern from electrons backscattered off Ag atoms. This can also be seen in Fig. 4 (b): The Sn emitter located below the molecular plane but on top of the substrate gives no signal that can be attributed to the substrate structure. Calculating a scattering pattern for a cluster with the molecule in the flattened adsorption geometry but without the Ag substrate confirms this finding (not shown).

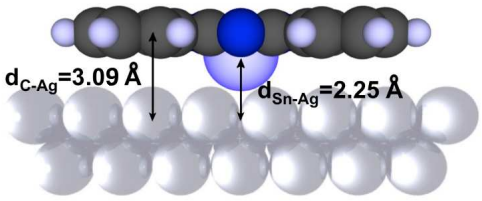

FIG. 5. Illustration of the adsorption geometry of the flattened SnPc on Ag(111) in an arbitrary adsorption site.

The three-fold symmetry of the substrate surface leads to the coexistence of three different azimuthal orientations of the adsorbed molecules, rotated by $\Delta\phi = 120°$

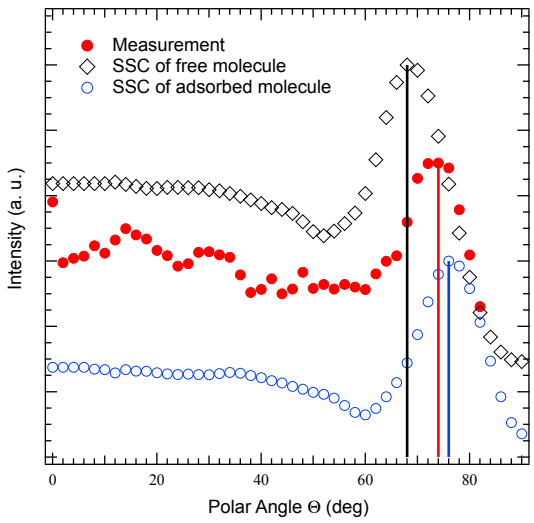

FIG. 6. ϕ-averaged polar intensity distribution of the results from Fig. 4. The measured XPD pattern (red filled circles), the SSC patterns from a molecule in the adsorbed (flat) geometry (blue open circles) and in the free (shuttlecock) geometry (black open diamonds) are shown. For the sake of clarity a vertical offset was added to each spectrum.

with respect to each other. Accordingly, to obtain the pattern shown in Fig. 4 (c), the result from Fig. 4 (b) was rotated twice by $\Delta\phi = 120°$ and the average of all three orientations was plotted. This reproduces the 12 main maxima found in the XPD measurements. Comparison of the experimental patterns in Figs. 4(f) and (g) with the SSC simulation in Fig. 4(c) reveals an azimuthal offset of $\phi = 15°$ for the 12 outer maxima between experiment and simulation. A rotation of the molecule in the cluster of $\Delta\phi = 15°$ relative to the Ag(111) surface, as illustrated in Fig. 4(g), reveals that the molecules preferentially align the diagonal vertical molecular mirror plane σ_v^d [see Fig. 4 (g)] along the dense rows of Ag atoms. Taking this rotation into account, the 12 main maxima appear at the same azimuthal and polar region as in the measurement. A similar rotational orientation was proposed by Stadler[26] and was also found in STM experiments.[16]

Additional information about the degree of order within the molecular layer can be gained by comparing the anisotropy $A = (I_{\max} - I_{\min})/I_{\max}$ between the experimental and the simulated data, as a measure for the diffraction contrast. Here, $I_{\max}$ is the intensity on a diffraction peak, and $I_{\min}$ the averaged intensity of the two adjacent minima along the azumuthal direction. For the peak labeled α at $\theta = 74°$ in Fig. 4(f) we calculated $A = 0.17$. For each of the maxima in Fig. 4(c) the anisotropy is A=0.47. The reasons for the smaller value in the experiment are as follows: (i) incomplete subtraction of the inelastic electron background from the experimental data can easily reduce the anisotropy; (ii) due to uncertainties in the treatment of thermal vibrations of the scatterers relative to the emitter, the SSC calculations tend to show larger anisotropies;[27] (iii) in the experiment some molecules might not be perfectly aligned in the geometry as shown in Fig. 4(h), which also reduces the experimental anisotropy.

Summarizing, in this section it is shown that with XPD the geometry of the system SnPc/Ag(111) can be characterized, leading to structural conclusions that are consistent with the existing literature. The polar position of the dominant scattering features in the intensity distribution shows that the molecular backbone of SnPc is flattened upon adsorption and that the Sn atom moves closer to the molecular plane. The distance between Sn-atom and molecular plane was determined to be 0.84 Å. The distance between the Sn atom and the Ag surface could not be found with XPD due to the lack of backscattering features. From the azimuthal position of the intensity maxima the azimuthal orientation of the molecules with respect to the Ag surface could be found: The diagonal vertical mirror plane σ_v^d of SnPc, is aligned with the direction of dense atomic rows of Ag atoms.

V. UV PHOTOELECTRON DIFFRACTION

For the same system of 0.9 ML SnPc on Ag(111) also UPD measurements were performed. The goal was to

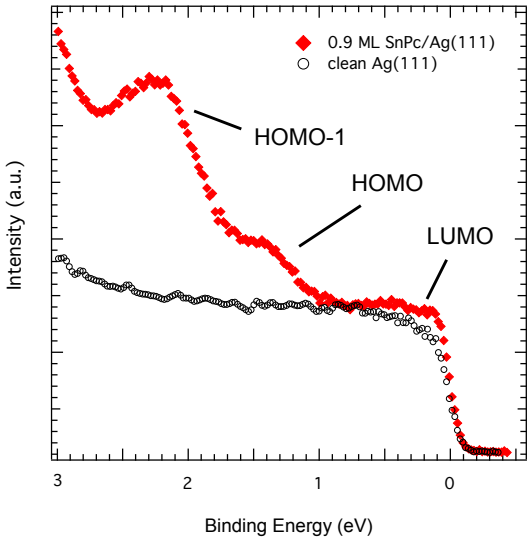

FIG. 7. UPS spectra near E_F excited with He I radiation ($h\nu = 21.2$ eV) of pristine Ag(111) (black open circles) and of 0.9 ML SnPc/Ag(111) (red diamonds) showing the highest occupied molecular states (see text for labeling of states). The latter spectrum was recorded at normal emission, while the clean surface spectrum was measured $\Delta\theta = 5°$ away from normal in order to avoid the surface state appearing close to E_F.[28]

demonstrate the sensitivity of low kinetic energy photoelectron diffraction patterns to molecular adsorbate structures, and the potential power of such measurements with respect to structural changes. Due to a much higher probability for backscattering, not only azimuthal orientation and conformational structure of the molecule, but also the molecule-substrate distance and bond lengths can potentially be extracted. However, the interpretation of UPD patterns is much less straightforward than in the case of XPD. The higher complexity of the initial states and of the scattering processes producing the UPD patterns demand a more elaborate theoretical treatment. Molecular orbital initial states in the valence region are more complex than spherically symmetric core states. Moreover, the muffin tin approximation becomes less accurate for slow electrons, and the surrounding potential in which the photoelectrons move is more difficult to compute compared to the XPD case.

To excite the HOMO-1 molecular orbital in the UPD measurement, He I_α radiation ($h\nu = 21.2$ eV) was used. In Fig. 7 the valence region of the system SnPc/Ag(111) as well as of the clean Ag(111) substrate is shown. The spectrum of SnPc/Ag(111) shows three peaks that correspond to molecular orbitals. The extra intensity observed right at the Fermi edge indicates emission from the LUMO. Due to charge transfer from the surface to the molecule this state is partially occupied when the molecule is adsorbed on a Ag(111) surface.[15] The two peaks at binding energies of 1.35 eV and 2.2 eV correspond to emission from the HOMO and HOMO-1, respectively. A DFT calculation with TURBOMOLE (*cf.* section IV) of the spatial distribution of these two orbitals in a free molecule is shown in Fig. 8 . The HOMO-1 has a pronounced s- and p_z-like character and is mainly localized around the Sn-atom of the molecule. In order to have a relatively simple molecular initial state that could be reasonably approximated by a single atomic orbital (a p_z orbital localized on the Sn atom), we chose the HOMO-1 state as emitter. It provides also the strongest signal-to-background ratio in the spectrum.

Figure 9 (b) shows the experimental UPD pattern of the HOMO-1 of SnPc/Ag(111) after subtraction of the substrate-related background, which has been measured at the same binding energy on pristine Ag(111) [see Fig. 9(a)]. The sharp contours in this background arise due to the strongly dispersing *sp* band of Ag moving through the binding energy window. They represent a section through a constant energy surface in the band structure of silver.[29] Due to their sharpness, and due to the dependence of the precise momentum mapping on the work function of the surface, some features persist in the background subtracted HOMO-1 UPD pattern, where they can be easily recognized. Due to the sensitivity of the molecules to radiation damage, UPD patterns were recorded only up to polar angles of $\theta = 60°$. This region includes the features with the highest anisotropy and thus the main information can be gained from this limited solid angle.

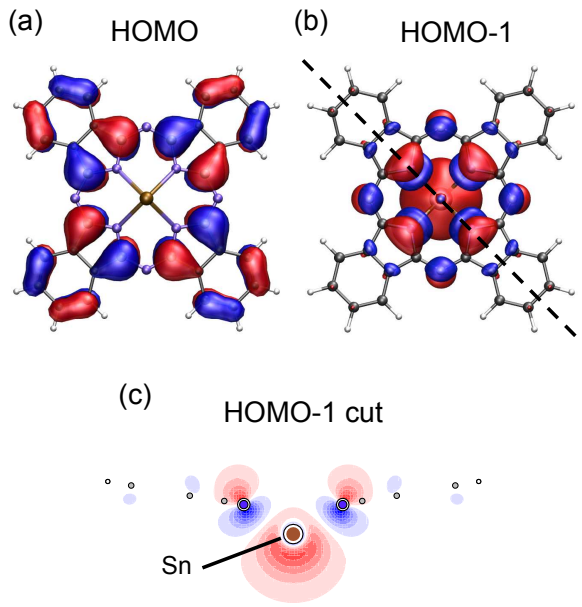

FIG. 8. The upper two pictures show a top view of the "tin-down" conformation of SnPc for the HOMO in (a) and the HOMO-1 in (b). (c) shows a cut through the HOMO-1 ("tin-down") in the vertical plane indicated by the dashed line in (b). The prominent Sn p_z-contribution to the HOMO-1 can be seen. The negative part of the p_z-orbital above the Sn-atom is missing due to the hybridization with the s-orbital localized on the same atom.

As in the XPD measurement a ring of 12 intensity maxima is observed, which are significantly broader and appear at a smaller polar angle of $\theta = 50°$ [see label α in Fig. 9(b)]. Again, the 12 maxima can be rationalized in terms of the four-fold rotational symmetry of SnPc placed on a three-fold symmetric substrate. But in contrast to the XPD data, a distinct three-fold symmetric modulation is superimposed on the 12 maxima. At lower polar angles ($\theta = 25°$) (label β) three bright maxima appear, partly intersected by a sharp ring-like artifact from the incomplete background subtraction. At normal emission a pronounced peak appears.

Figure 9(c) shows the best fit that we could achieve with SSC simulations for emission from the HOMO-1, excited with He I_α radiation. Due to the large Sn p_z contribution to the HOMO-1, the emitter is approximated by a p_z-orbital centered at the Sn atom. Later this fact will be discussed in more detail (see also APPENDIX). In the resulting SSC pattern the maximum in normal emission as well as the three bright maxima at $\theta = 25°$ (label δ) are well reproduced. Moreover, the figure shows that the three-fold symmetry of the substrate clearly dominates over the 12-fold symmetry expected from intramolecular scattering from a four-fold symmetric molecule adsorbed in three coexisting orientations. This is in clear contrast to the XPD case. An SSC simu-

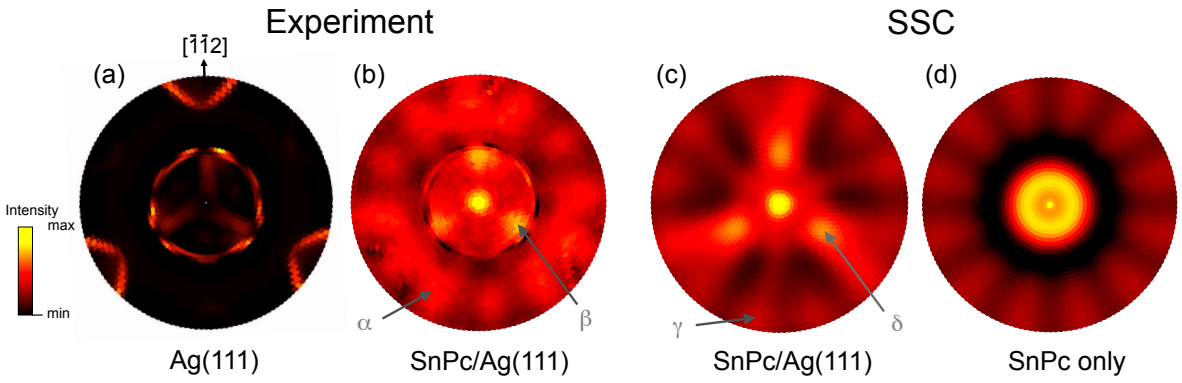

FIG. 9. UPD measurements and corresponding SSC calculations. (a) Experimental angular intensity map for the energy region $E_B = 2.3$ eV from a clean Ag(111) substrate, serving as a reference for the anisotropies in the spectral background; (b) UPD measurement of the HOMO-1 of a 0.9 ML film of SnPc on Ag(111), with the background anisotropy removed as much as possible. Additionally a Gaussian shaped background was subtracted. (c) Average pattern of 20 three-fold symmetrized SSC simulations of a cluster containing the atoms of the SnPc molecule and 2 layers of Ag(111). Each of the 20 simulations result from a cluster where the molecule is adsorbed on a different lateral adsorption site (see text). (d) SSC simulation of a SnPc molecule in the adsorbed geometry without the Ag substrate. All plots cover a polar angle range going from normal emission ($\theta = 0°$, center of the plot) to $\theta_{\max} = 60°$ (outer rim).

lation of a SnPc molecule without substrate is shown in Fig. 9(d), yielding 12 equally intense maxima after three-fold averaging. The superimposed three-fold symmetry in Fig. 9 (c) can thus be attributed to backscattering of photoelectrons from substrate atoms in the vicinity of the molecule, which is more pronounced for low-kinetic energy electrons. (*cf.* Fig. 1). It is remarkable that this three-fold symmetry persists even after averaging over 20 inequivalent adsorbate positions within the Ag(111) surface unit cell.

Comparing the experimental UPD pattern and the SSC simulation in Figs. 9 (b) and (c), respectively, reveals that the simulations slightly overestimate the amount of backscattering as the relative intensity of the bright inner features vs. the 12 outer maxima is higher in the simulated pattern. This is also confirmed by a comparison of the anisotropy for the outer (label α) and inner (label β) maxima in the measured UPD pattern and in the simulated UPD (label γ *vs.* δ), respectively. Table I shows that the ratio between the anisotropies of the outer and inner maxima is smaller for the calculated than for the measured data.

	Experimental	Calculated
Outer max.	A(α)=0.13	A(γ)=0.07
Inner max.	A(β)=0.15	A(δ)=0.13

TABLE I. Anisotropies for selected outer and inner maxima (*cf.* labels in Fig. 9) in in the experimental and in the calculated UPD pattern, respectively.

The 12 outer maxima, which are due to intramolecular scattering in the SnPc backbone, appear at similar polar angles in both simulation ($\theta = 54°$, labeled δ) and experiment ($\theta = 50°$, labeled β). This slight inward shift of the experimental pattern with respect to the SSC simulation for the flat SnPc backbone is consistent with the result from the XPD analysis and might indicate that a slight bending of the molecule into a shuttlecock conformation persists in the adsorbed state.

Having clearly established the contribution of backscattering to the formation of the UPD pattern, one would like to explore its sensitivity to the bond distance of the molecule from the substrate. This was realized by including the first two layers of Ag atoms in the cluster and varying the vertical distance between molecule and top Ag layer. The best fit [Fig. 9 (c)] was achieved with very similar structural parameters ($d_{\text{Sn-Ag}} = 2.30$ Å, $d_{\text{C-Ag}} = 3.09$ Å) as used in the XPD simulations. To account for the incommensurate superstructure, the same grid with 20 different adsorption sites of the SnPc molecules on the Ag unit cell was used as already mentioned in section IV. A three-fold average was carried out to account for the three rotational Ag(111) domains. In Fig. 10 we show a series of SSC patterns for the HOMO-1 emission in which the distance between molecules and substrate $d_{\text{Sn-Ag}}$ was varied. In Fig. 10 (a) the distance between SnPc and substrate is the smallest, three additional spots appear in-between the three inner maxima (label ε). These spots gradually vanish as the molecule is moved further away from the Ag surface [see Figs. 10(b) through (d)]. In the case of our best fit with $d_{\text{Sn-Ag}} = 2.30$ Å [see Fig. 9(c)] both, the three maxima at $\theta = 25°$ and the additionally appearing maximum at normal emission are strong. Upon further increasing the molecule-substrate distance the three-fold symmetric fingerprint of the substrate declines while the emission

normal to the surface becomes stronger. On a scale of sub-angstrom distance variations the UPD pattern changes significantly, which makes such measurements a very sensitive probe for structural changes. The molecule-substrate distance determined from our best fit is in good agreement with the XSW measurements by Stadler *et al.*[12]

Simulating UPD patterns is generally more challenging than the XPD case for mainly three reasons: (i) the non-spherical and hybridized character of the initial state wave functions, (ii) the non-local character of molecular orbital states leading to coherent photoemission from multiple atoms within the same molecule, and (iii) the lack of an accurate description of the scattering potentials as well as the inner potential V_0 within molecular layers. These issues complicate the calculation of photoemission matrix elements and scattering phase shifts for the photoelectrons. Only just recently have these issues been addressed in the literature[4]. In this work we have tackled issues (i) and (iii) at least partly.

It is obvious that the approximation of the HOMO-1 as a p_z orbital localized on the Sn atom is a crude one. A next better approximation would be an *sp*-hybridized orbital, and then the full molecular orbital as depicted in Fig. 8. Moreover, the HOMO-1 likely plays an important role in the chemisorption process between the first monolayer of molecules and the silver substrate.[12,14] Charge donation and back-donation can lead to a change in the spatial distribution of the HOMO-1, as it was recently suggested based on DFT calculations with a semi-empirical dispersion correction.[14] The good agreement of the single scattering calculations assuming a p_z-emission

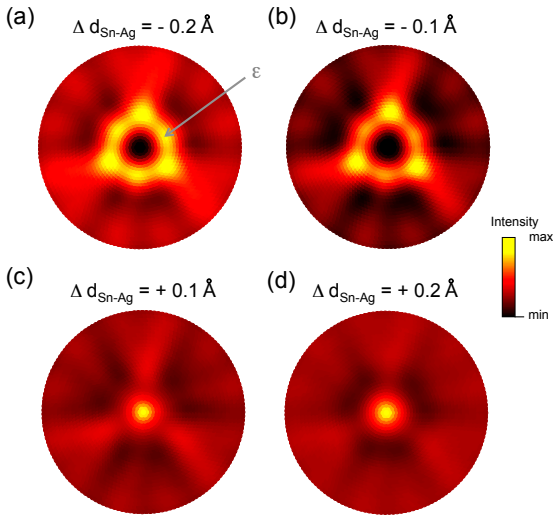

FIG. 10. SSC simulations of the HOMO-1 UPD pattern using a p_z-type emitter for different molecule-substrate distances with distance offsets $\Delta d_{\text{Sn-Ag}}$ referenced to the best fit distance $d_{\text{Sn-Ag}} = 2.30$ Å. The polar angle range goes from $\theta = 0°$(center of plots) to $\theta_{\max} = 60°$ (outer border of plots).

with the experimental data [Figs. 9 (b) and (c)] suggests that the p_z-orbital character of the HOMO-1 remains dominant and largely unchanged upon adsorption. This statement is also supported by our own DFT calculations.

With a work function of $\phi = 4.4$ eV,[30] the kinetic energy of photoelectrons from the HOMO-1 in vacuum is $E_{kin} = 14.6$ eV when excited with He I_α radiation. Due to calculations with the self-consistent LMTO approach the inner potential, which is required for the calculation of phase shifts for scattering inside the solid, was assumed to be $V_0 = 8.7$ eV for SnPc/Ag(111).[31] In the present case we introduce V_0^{eff} instead of V_0 and use it as a fitting parameter as electrons from the top-most molecular layer do not experience the same inner potential as those inside the solid. The best fit of the SSC results to the experimental UPD pattern was achieved with $V_0^{\text{eff}} = 6.0$ eV. This procedure even enlarged the parameter space that had to be converged, which was already spanned by the geometrical degrees of freedom such as substrate-molecule distance and the molecule geometry itself. Our own XPD measurements and XSW data from the literature, however, provided a good starting point for the structural parameters.
In consideration of the discussed difficulties the presented SSC result in Fig. 9 (c) shows a remarkably good agreement with the measured pattern.

VI. SUMMARY

We have examined the system SnPc/Ag(111) with a coverage of 0.9 ML of SnPc with XPD and UPD measurements. From the XPD analysis, supported by SSC calculations, the conformation of the SnPc molecules on Ag(111) could be determined. The slightly shuttlecock shaped molecule experiences a flattening, while the Sn atom sticking out beneath the molecular plane moves a little closer. Furthermore, comparing SSC calculations and experimental data for both, Sn $3d_{5/2}$ and Ag $3d_{5/2}$, it is found that the diagonal vertical mirror plane σ_v^d of SnPc aligns with the Ag(111) unit cell vector, *i.e.* with dense rows of Ag atoms. These results confirm earlier findings.[16,26]

This knowledge was taken into account for the analysis of our UPD data from the same system. To simulate emission from a molecular state, *i. e.* the HOMO-1, the SSC code was adapted so that it can calculate photoelectron diffraction patterns also from non-spherically symmetric states, such as a p_z-state. Although the processes involved in forming a UPD pattern are far more complex than in the XPD case, a good agreement between SSC simulations and our UPD data could be obtained for a molecule-substrate distance of $d_{Sn-Ag} = 2.30$ Å and $d_{C-Ag} = 3.09$Å, again in good agreement with XSW data.[12] With a series of SSC calculations where the molecule-substrate distance was varied, it could be shown that UPD is a powerful method to detect struc-

tural changes of surfaces on a sub-angstrom scale. The sensitivity of the analysis to the parameter d_{Sn-Ag} results from strong backscattering contributions from Ag atoms which are essentially absent in the XPD case.

As photoelectrons emitted from a molecular monolayer experience another inner potential compared to those propagating in the bulk, also the inner potential was adjusted. A best fit was found at a value of $V_0^{\text{eff}} = 6.0$ eV. The uncertainties of the inner potential, as well as the sensitivity of the calculated UPD patterns to even small changes in scattering phase shifts and photoemission matrix elements, demand an increased theoretical effort in the future, also including a multiple scattering treatment.[4,11]

The findings of this work are particularly encouraging in view of the increasing availability of ultrashort XUV laser pulses from HHG sources.[5] A pump-probe scheme becomes feasible where a molecular layer is excited by a strong infrared pump pulse and a subsequent XUV pulse is used for recording a UPD pattern to follow the structural evolution of the system as a function of the pump-probe delay, *i.e.* in the femtosecond regime. Processes involved in reversible molecular switches or in molecular desorption may become directly accessible to stroboscopic measurements.

VII. ACKNOWLEDGEMENT

We would like to thank Peter Krüger and Moritz Hoesch for theoretical support and fruitful discussions. Financial support of the Swiss National Science Foundation through the NCCR-MUST is gratefully acknowledged.

A. APPENDIX

The simulation of UPD patterns required a modification of our existing SSC code to account at least partly for the molecular orbital character of the initial states. We extended the code so that it can calculate not only diffraction patterns for emission from completely filled core states with spherical symmetry, but also from anisotropic states with defined angular momentum and magnetic quantum numbers, *e. g.*, a p_z-orbital. As previously mentioned, the latter was used as emitter for the simulation of the UPD pattern in Fig. 9 (c). Calculations with emission from an *s*-state were also performed, but could not reproduce the features observed in the experimental data.

To show the validity of the extended code for scattering from non-isotropic emitters, a case with a simple emitter-scatterer configuration is presented in Fig. 11. The cluster consists of a Sn photoemitter and three carbon scatterers, one along each of the three Cartesian axes, as sketched in Fig. 11 (c). Diffraction patterns for emission from three orthogonal *p*-states (p_x, p_y and p_z)

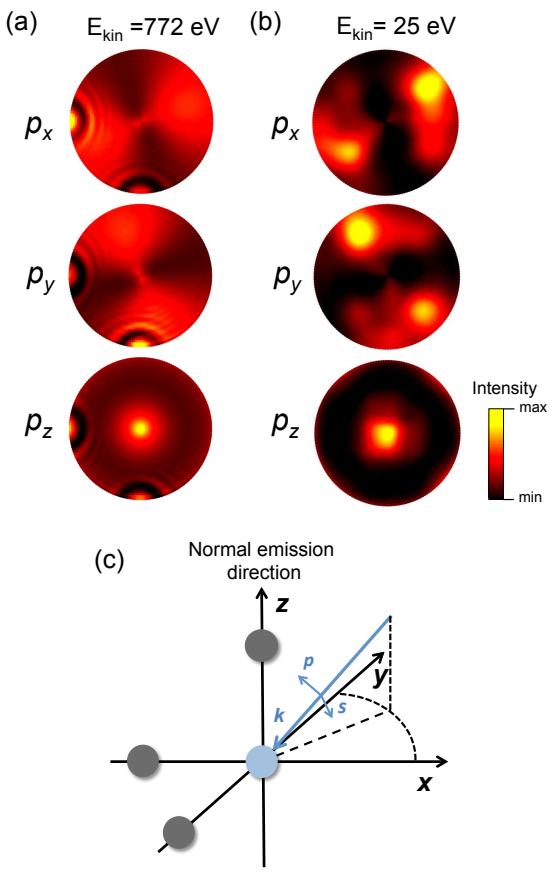

FIG. 11. (a) SSC simulation of intensity patterns for emission from three orthogonal *p*-orbitals ($E_{kin} = 772$ eV in the solid). From top to bottom: p_x, p_y and p_z for the simple three-scatterer geometry depicted in (c). (b) SSC simulation as in (a) but with $E_{kin} = 25$ eV in the solid. The polar angle ranges from $\theta = 0^\circ$ (center of the plots) to $\theta_{\max} = 86^\circ$ (outer border of plots). (c) The corresponding three carbon scatterer geometry shown in a cartesian coordinate system. Situated in the coordinate origin is a Sn-emitter. The blue arrow indicates the direction of light incidence with s- and p-polarizations.

were then calculated. In Fig. 11 (a) the kinetic energy of the electrons was chosen as in the XPD experiment. In Fig. 11 (b) we assumed E_{kin} to be the same as in the UPD experiment. The experimental geometry, *i.e.* the direction of incident light and detection axis, were assumed to be the same as in our real UPD experiment for both examples in (a) and (b). The incident light is partially polarized and has contributions from s and p polarization.

In Fig. 11 (a) the higher kinetic electron energy facilitates the direct interpretation of the diffraction pattern. As expected the symmetry of the initial state greatly determines the outcome of the scattering: emission from a p_z-initial state shows a pronounced emission and forward scattering along the *z*-axis, *i. e.* in the normal emission direction (the center of the picture). Likewise

emission from a p_x initial state shows a pronounced emission and forward scattering in the x-axis direction. It is thus demonstrated that the modified SSC code also accounts for non-spherically-symmetric emitters. Figure 11 (b) illustrates that an intuitive interpretation of UPD patterns is not possible. Due to large phase shifts and a complicated scattering character of the low-energy electrons the diffraction pattern depicts the scatterer and the initial state geometry only very vaguely.

[1] J. Osterwalder, in *Surface Analysis by Auger and X-Ray Photoelectron Spectroscopy*, edited by D. Briggs and J. Grant, p. 557 ff., (IM Publications and Surface Spectra Limited, 2003).

[2] D. Naumovic, A. Stuck, T. Greber, J. Osterwalder, and L. Schlapbach, Phys. Rev. B **47**, 7462 (1993).

[3] R. Fasel, J. Wider, C. Quitmann, K.-H. Ernst, and T. Greber, Angew. Chem. Int. Ed. **43**, 2853 (2004).

[4] M. Shang *et al.*, J. Electron. Spectrosc. Relat. Phenom. **184**, 261 (2011).

[5] C. Spielmann *et al.*, Science **278**, 661 (1997).

[6] P. Puschnig *et al.*, Science **326**, 702 (2009).

[7] P. Puschnig *et al.*, Phys. Rev. B **84**, 235427 (2011).

[8] J. Ziroff, F. Forster, A. Schöll, P. Puschnig, and F. Reinert, Phys. Rev. Lett. **104**, 233004 (2010).

[9] S. Kono, S. M. Goldberg, N. F. T. Hall, and C. S. Fadley, Phys. Rev. B **22**, 6085 (1980).

[10] J. Osterwalder, T. Greber, P. Aebi, R. Fasel, and L. Schlapbach, Phys. Rev. B **53**, 10209 (1996).

[11] P. Krüger, F. Da Pieve, and J. Osterwalder, Phys. Rev. B **83**, 115437 (2011).

[12] C. Stadler, S. Hansen, I. Kröger, C. Kumpf, and E. Umbach, Nat. Phys. **5**, 153 (2009).

[13] C. Stadler *et al.*, Phys. Rev. B **74**, 035404 (2006).

[14] J. D. Baran and J. A. Larsson, J. Phys. Chem. C , 9487 (2012).

[15] M. Häming, C. Scheuermann, A. Scholl, F. Reinert, and E. Umbach, J. Electron. Spectrosc. Relat. Phenom. **174**, 59 (2009).

[16] M. Toader and M. Hietschold, J. Phys. Chem. C **115**, 12494 (2011).

[17] M. Toader and M. Hietschold, J. Phys. Chem. C **115**, 3099 (2011).

[18] J. B. Pendry, Low energy electron diffraction, Academic Press London and New York, 1974.

[19] R. Clementi and C. Roetti, Atomic Data and Nuclear Data Tables **14**, 177 (1974).

[20] S. Goldberg and C. Fadley, J. Electron. Spectrosc. Relat. Phenom. **21**, 285 (1981).

[21] Y. Chen and M. A. van Hove, MSCD photoelectron diffraction program package, Private Communications .

[22] T. Greber *et al.*, Rev. Sci. Instrum , 4549 (1997).

[23] G. Attard and C. Barnes, *Surfaces* (Oxford University Press, 1998).

[24] TURBOMOLE V6.3.1 2011, a development of University of Karlsruhe and Forschungszentrum Karlsruhe GmbH, 1989-2007, TURBOMOLE GmbH, since 2007; available from `http://www.turbomole.com`.

[25] C. Adamo and V. Barone, J. Chem. Phys. **110**, 6158 (1999).

[26] C. Stadler, *Strukturuntersuchungen organischer Monolagen auf Ag(111)*, PhD thesis, University of Würzburg, 2009.

[27] R. Fasel *et al.*, Surf. Sci. **374**, 104 (1996).

[28] F. Reinert, G. Nikolay, S. Schmidt, D. Ehm, and S. Hüfner, Phys. Rev. B **63**, 115415 (2001).

[29] P. Aebi, J. Osterwalder, R. Fasel, D. Naumovic, and L. Schlapbach, Surf. Sci. **307-309**, 917 (1994).

[30] M. Häming, M. Greif, C. Sauer, A. Scholl, and F. Reinert, Phys. Rev. B **82**, 235432 (2010).

[31] O. K. Andersen, Z. Pawlowska, and O. Jepsen, Phys. Rev. B **34**, 5253 (1986).